Glider Observations of Sediment Resuspension in a Middle Atlantic Bight Fall Transition Storm

8 authors, including:

Scott Glenn
Rutgers, The State University of New Jersey
243 PUBLICATIONS   **4,089** CITATIONS

Michael Twardowski
Harbor Branch Oceanographic Institute, Florida Atlantic University
117 PUBLICATIONS   **4,151** CITATIONS

Louis Bowers
Rutgers, The State University of New Jersey
16 PUBLICATIONS   **139** CITATIONS

Josh Kohut
Rutgers, The State University of New Jersey
163 PUBLICATIONS   **2,103** CITATIONS

Some of the authors of this publication are also working on these related projects:

Project   Links Between Coastal Hydrodynamics and Plankton Assemblages View project

Project   EEGLE: Episodic Events in the Great Lakes Experiment View project

Glider observations of sediment resuspension in a Middle Atlantic Bight fall transition storm

Scott Glenn
Coastal Ocean Observation Lab, Institute of Marine and Coastal Sciences, School of Environment and Biological Sciences, Rutgers University, New Brunswick, New Jersey, 08901, http://marine.rutgers.edu/cool

Clayton Jones
Webb Research Corporation, 82 Technology Park Drive, East Falmouth, Massachusetts, 02536-4441

Michael Twardowski
WET Labs, Inc., Department of Research, 165 Dean Knauss Drive, Narragansett, Rhode Island, 02882

Louis Bowers, John Kerfoot, and Josh Kohut
Coastal Ocean Observation Lab, Institute of Marine and Coastal Sciences, School of Environment and Biological Sciences, Rutgers University, New Brunswick, New Jersey, 08901, http://marine.rutgers.edu/cool

Doug Webb
Webb Research Corporation, 82 Technology Park Drive, East Falmouth, Massachusetts, 02536-4441

Oscar Schofield
Coastal Ocean Observation Lab, Institute of Marine and Coastal Sciences, School of Environment and Biological Sciences, Rutgers University, New Brunswick, New Jersey, 08901, http://marine.rutgers.edu/cool

Abstract

In October of 2003 a fleet of autonomous underwater gliders began a time series of transects across the New Jersey shelf. The gliders are equipped with a conductivity–temperature–depth sensor, and some carry optical ECO-sensor pucks. The physical–optical data are used to examine storm-induced sediment resuspension. There are two types of storm response found. In summer, the seasonal stratification limits midshelf sediment resuspension to below the pycnocline even during hurricanes. In contrast, winter storms suspend sediment throughout the full water column. The transition between summer and winter seasons starts with surface cooling that preconditions the shelf for rapid mixing during fall storms. The mixing storm of October 2003 was a classic northeaster. Early in the storm when waves were high, sediment resuspension was limited to below the pycnocline. After the pycnocline eroded through growth of the bottom boundary layer, particles immediately filled the full water column. The spectral ratio of backscatter indicated that the particles were likely similar materials both before and after the stratification was eroded. The backscatter profiles in the bottom boundary layer decay with distance from the bed at rates consistent with theory but with variable slopes. The reduced slope of the backscatter profiles increased after stratification was lost, which is consistent with an increase in vertical transport or turbulent mixing. Wave bottom orbital velocities during this time were decreasing, and the glider vertical velocities showed no enhancement consistent with Langmuir cells. Enhanced mixing was related to the interaction of the surface and bottom boundary layers while the stratification was eroded, and the observed variability in the resuspension during the event was also due to the tide.

Storm-driven mixing events are episodic but important physical processes in the oceans (Wiggert et al. 2000; Chang et al. 2001; Zedler et al. 2002). It is known that these events play an important, but as yet poorly quantified, role in the ecosystem dynamics of the ocean (Babin et al. 2004). Mixing events are especially significant on continental shelves, where storm events can affect the full water column and the sediment bed below (Chang et al. 2001). Yet traditional sampling techniques are limited by the extreme conditions experienced in storms, biasing observations to fair weather conditions.

The Middle Atlantic Bight (MAB) experiences severe tropical and extratropical coastal storms during the

Report Documentation Page

Form Approved
OMB No. 0704-0188

Public reporting burden for the collection of information is estimated to average 1 hour per response, including the time for reviewing instructions, searching existing data sources, gathering and maintaining the data needed, and completing and reviewing the collection of information. Send comments regarding this burden estimate or any other aspect of this collection of information, including suggestions for reducing this burden, to Washington Headquarters Services, Directorate for Information Operations and Reports, 1215 Jefferson Davis Highway, Suite 1204, Arlington VA 22202-4302. Respondents should be aware that notwithstanding any other provision of law, no person shall be subject to a penalty for failing to comply with a collection of information if it does not display a currently valid OMB control number.

1. REPORT DATE **2008**	2. REPORT TYPE	3. DATES COVERED **00-00-2008 to 00-00-2008**

4. TITLE AND SUBTITLE **Glider observations of sediment resuspension in a Middle Atlantic Bight fall transition storm**	5a. CONTRACT NUMBER
	5b. GRANT NUMBER
	5c. PROGRAM ELEMENT NUMBER
6. AUTHOR(S)	5d. PROJECT NUMBER
	5e. TASK NUMBER
	5f. WORK UNIT NUMBER

7. PERFORMING ORGANIZATION NAME(S) AND ADDRESS(ES) **Rutgers University,Coastal Ocean Observation Lab,Institute of Marine and Coastal Sciences,New Brunswick,NJ,08901**	8. PERFORMING ORGANIZATION REPORT NUMBER

9. SPONSORING/MONITORING AGENCY NAME(S) AND ADDRESS(ES)	10. SPONSOR/MONITOR'S ACRONYM(S)
	11. SPONSOR/MONITOR'S REPORT NUMBER(S)

12. DISTRIBUTION/AVAILABILITY STATEMENT
Approved for public release; distribution unlimited

13. SUPPLEMENTARY NOTES

14. ABSTRACT
see report

15. SUBJECT TERMS

16. SECURITY CLASSIFICATION OF:			17. LIMITATION OF ABSTRACT	18. NUMBER OF PAGES	19a. NAME OF RESPONSIBLE PERSON
a. REPORT **unclassified**	b. ABSTRACT **unclassified**	c. THIS PAGE **unclassified**	**Same as Report (SAR)**	**17**	

Standard Form 298 (Rev. 8-98)
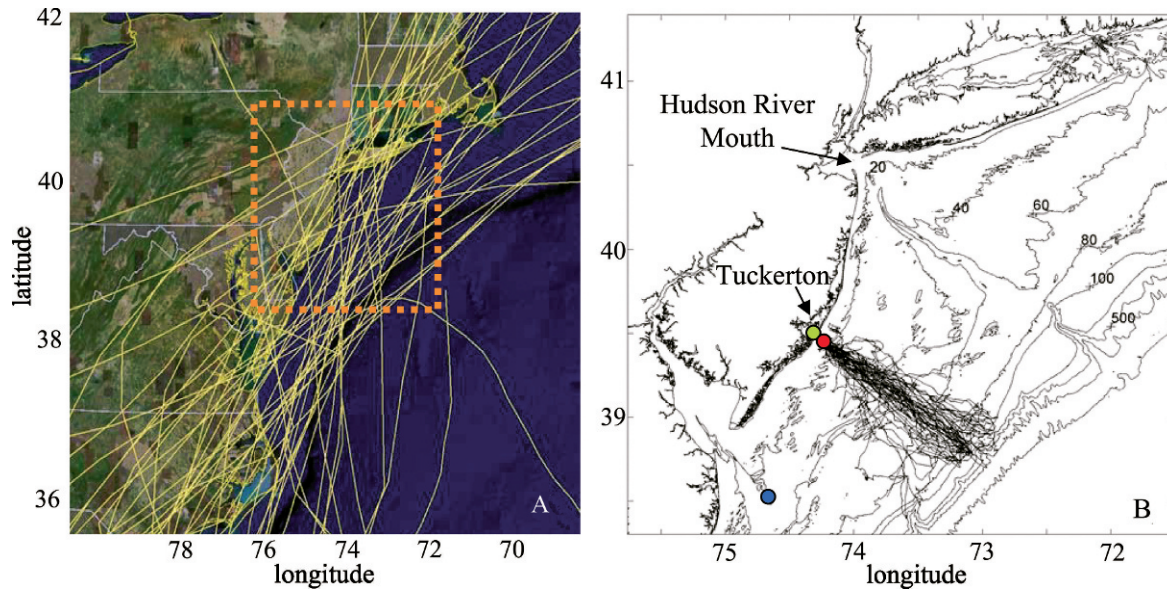Prescribed by ANSI Std Z39-18

Fig. 1. (A) All recorded hurricane and tropical storm tracks passing within 100 km of the Tuckerton, New Jersey, study site since 1900. (B) Observatory sampling locations used in this study, including the Tuckerton glider endurance line (blue lines), Long-term Ecosystem Observatory (LEO) (red circle), the Tuckerton Meteorological Tower (green circle), and the NOAA Delaware Bay weather buoy (blue circle).

summer and early autumn (Colle 2003; Evans and Hart 2003; Jones et al. 2003; Landreneau 2003). These seasonal storms often track along a corridor running parallel to the coast between the shelf break and several tens of kilometers inland (Fig. 1A). In late autumn and winter months severe northeasters are formed through rapid cyclogenesis associated with the Gulf Stream off Cape Hatteras (Sanders and Gyakum 1980; Nielsen and Dole 1991; Keim et al. 2004). In addition to the significant human safety issues associated with these storms, they play a disproportionately large role in the transport of particulate material on the continental shelf (Keen et al. 1994; Styles and Glenn 2005).

Sediment transport processes on continental shelves are often characterized in terms of the turbulent interactions between combined wave and current flows (Grant and Madsen 1979). High bottom shear stress associated with the thin oscillatory wave boundary layer acts to mobilize the sediment so that it is available for transport by the mean currents. The combination is an efficient sediment transport mechanism, since the turbulence associated with the thicker pure current boundary layer may not be sufficient to initiate sediment motion and, to first order, the oscillatory motion of the waves results in little net sediment transport. In cases when the waves and currents are strong enough to suspend bed sediment in the water column, the process is often modeled as a Fickian balance between the tendency of the turbulence to lift sediment above the bed and the countertendency of the sediment fall velocity to return it (Smith and McLean 1977; Glenn and Grant 1987). In the absence of sediment induced self-stratification, the balance results in a standard Rouse profile where the suspended sediment concentration decays with distance from the seabed at rates that appear constant on log–log scales.

Tides with timescales shorter than the typical northeaster are expected on a theoretical basis to impact the temporal

characteristics of sediment transport and deposition patterns during MAB storms (Keen and Glenn 1994, 1995). In these cases, strong winds from the northeast result in a downwelling condition, where transport near the bed is predominantly alongshore but with a cross-shore component in the offshore direction. In their model results, the smaller cross-shore component was similar in magnitude to the predominantly cross-shore tides, resulting in little cross-shore transport on an incoming tide and, owing to the nonlinear interactions of the turbulence scales, significantly more offshore transport during outgoing tides. The resulting nonzero average tidal contribution enhances the offshore transport during the northeaster.

Comprehensive understanding of these interactions were expanded as studies incorporated the time-varying seafloor ripple roughness (Traykovski et al. 1999; Styles and Glenn 2002; Traykovski 2007), wave-current interactions, and suspended sediment induced stratification (Styles and Glenn 2000). Styles and Glenn (2005) used a 2-y inner-shelf data set and applied the improved bottom boundary layer models during sediment transporting storms and found that the alongshore transport was southward as expected, but the cross-shore component of the observed transport was predominantly onshore at their measurement site. Thus despite the expectation that northeasters should produce downwelling circulation with offshore bottom transport that is reinforced by the tides, other local scale processes must be in effect. Some of the potential factors underlying these unknown processes include potential topographic interactions that operate over the relatively small (a few kilometers) scale of the ubiquitous ridge and swale topography of the MAB inner shelf (McBride and Moslow 1991), or over the larger (a few tens of kilometers) scale of the topographic highs that impact the location of summertime upwelling centers (Glenn et al. 2004b). Additionally, Gargett et al. (2004) identified full water

column Langmuir cells as a significant driver of sediment resuspension events at the same inner-shelf location. Finally, sediment transport patterns are also influenced by the vertical mixing of the resuspended sediment, which can be inhibited by stratification.

The MAB experiences seasonal warming, freshwater river inputs, and alongshelf transport from the north that result in a strong summer pycnocline (Beardsley and Boicourt 1981; Biscayne et al. 1994; Castelao et al. 2008). Summertime temperature differences of up to 15°C over depths of just a few meters are commonly observed. In contrast, the winter conditions are well mixed over the full water depth. The transition between stratified and well mixed usually occurs in late September or October and is most often associated with a storm mixing event rather than cooling of the surface that results in vertical overturning (Beardsley and Boicourt 1981). Even though the dominant southwest to northeast track of the winter and summer storms is similar, the strength of the seasonal pycnocline limits turbulent transport across the layer in summer. This suggests that the sediment transport response in summer and winter storms may be different due to the differences in stratification.

This study first examines data from summer and winter storms to identify the differences, and then focuses on a fall transition mixing storm to compare sediment resuspension during both weakly stratified and unstratified conditions. In order to study the spatial and temporal mechanisms of sediment resuspension and transport processes on the MAB continental shelf, we used autonomous Slocum gliders equipped with physical and optical sensors.

Materials and methods

This study was conducted in the Middle Atlantic Bight (MAB) off the New Jersey shore (Fig. 1B) in waters continuously monitored by a shelf-wide coastal ocean observatory (http://marine.rutgers.edu/cool; Schofield et al. 2002; Glenn and Schofield 2004). Satellites and high frequency radar provide spatial maps of the surface waters that are augmented with subsurface time series measurements made from the cabled Long-term Ecosystem Observatory (LEO) (Glenn et al. 2000) and a fleet of Slocum gliders (Glenn et al. 2004a; Schofield et al. 2007). Surface winds and waves are available from nearby weather buoys maintained by the National Oceanic and Atmospheric Association (NOAA) National Data Buoy Center, in particular, Sta. 44009, located offshore of Delaware Bay. Slocum gliders are a robust autonomous underwater scientific platform (Davis et al. 2003; Schofield et al. 2007) manufactured by Webb Research Corporation. They are 1.8-m long, torpedo-shaped, buoyancy-driven vehicles with wings that enable it to maneuver through the ocean at a forward speed of 20–30 cm s^{-1} in a sawtooth-shaped gliding trajectory. A full description of our scientific operation of the Slocum gliders can be found in Schofield et al. (2007).

Each Slocum glider has a payload bay that houses a SeaBird conductivity–temperature–depth sensor and includes space for a range of additional sensors. The glider acquires its global positioning system (GPS) location every time it surfaces, which early on was set at once per hour in 2003 and later extended to once every 6 h in 2004. By dead reckoning along a compass bearing while flying underwater, estimates of depth averaged current can be calculated based on the difference between the glider's expected surfacing location and the actual new GPS position. Depth averaged current measurements obtained in this manner have been validated against stationary acoustic Doppler current profiler data on programmed flybys (Glenn and Schofield 2004). These physical measurements are complemented with several different biooptical sensor options that often vary with each glider. The early gliders in the Rutgers fleet were outfitted with Hobi Labs HydroScat-2 sensors (http://www.hobilabs.com/); however, subsequent gliders have been equipped with dual WetLabs ECO-BB3 sensor pucks. These compact sensors have proved to be extremely stable with a wide dynamic range that spans most conditions encountered in our global deployments. The pucks provide spectral measurements of light backscatter along with the fluorescence of chlorophyll *a* (Chl *a*) and colored dissolved organic matter (CDOM).

The glider-based time series initiated in 2003 consists of a cross-shore endurance line that runs across the MAB shelf (Fig. 1B, Castelao et al. 2008). The inshore side of the glider endurance line starts at the Long-term Ecosystem Observatory located 10 km off the Tuckerton shore and extends offshore to about the 100-m isobath, stopping just inshore of the intense fishing activity encountered at the shelfbreak. The length of the Tuckerton glider endurance line is about 120 km. Since the glider's typical horizontal speed is about 1 km h^{-1}, it usually takes about 5 d to cross the shelf. The glider was programmed to undulate between 2 m below the surface and 2 m above the bottom, surfacing every hour for a new position fix and to transmit data to shore. Since the inflections at the surface or bottom require 10–20 s to complete, profiles can and often do extend closer to the bottom than 2 m. During each 1-h time interval below the surface, between five and seven profiles were collected, dependent on the water depth. To conserve power, data on the initial deployments were collected on downcasts only. The first dive from the surface is clearly observed in each hourly segment with the near surface expression in the glider data.

The glider data is complemented by both atmospheric data and forecasts. Observations from the NOAA weather buoys were combined with Rutgers onshore meteorological network (http://climate.rutgers.edu/njwxnet/) that included a meteorological tower at the coast near Tuckerton that provided observations of wind speed and direction, temperature, and barometric pressure. Weather forecasts using the weather research and forecast model (Skamarock et al. 2005) were generated. Operationally, several model domains are run throughout the course of a day for the MAB region. The domains included spatial resolutions of 18 km, 10 km with a nested 2.5-km grid, and 12 km with a 4-km nested grid. The 18-km and 10-km domains used boundary conditions from NOAA National Center for Environmental Prediction (NCEP) global forecast system, and the 12-km domain used boundary conditions from the NCEP North American model. Sea surface temperatures

from the NOAA 1/12° high-resolution real-time global analysis are used in the initialization of the model.

Results

The effect of stratification on resuspension—The long operational duration of autonomous underwater gliders, combined with their ability to continue sampling even during extreme weather, provides scientists a new platform for studying sediment transport processes during storms. In this example, each glider typically patrols the Tuckerton endurance line for 3–5 weeks at a time. Those gliders with payload bays equipped with optical backscatter sensors that respond to particles in suspension provide observations of sediment response with each passing storm. Because storm currents are often faster than the typical maximum glider forward speed of about 30 cm s^{-1}, each passing storm can be readily identified in the glider track data as a deviation from the alongshelf line. Two examples are illustrated in Fig. 2. Glider track maps (Fig. 2A and 2B) indicated that in both cases, the storm-induced currents (indicated by the vectors plotted along the track) were so strong the gliders could not maintain their cross-shelf transect. In each case, the glider's forward velocity was moving it cross-shelf to the southeast toward a distant offshore point, while the storm-driven currents moved it alongshore to the north (Fig. 2A) or south (Fig. 2B). The plots illustrate that the Lagrangian transport pathways during storms tend to be short, on the order 30 to 40 km during the most severe events.

The November 2003 northeaster (Fig. 2A) passed inshore of the glider, resulting in an alongshore drift to the north. On 14 November 2003, the northeaster resulted in Delaware Bay buoy wind speeds that peaked at 18 m s^{-1} with wave heights at 3.2 m, and peak periods of 6 s. The northeaster passed through the area while the glider was at about a depth of 25 m to 35 m, close to the midshelf. Temperature data from the glider (Fig. 2C) are typical for the unstratified winter season. The high optical backscatter from resuspended particles detected by the glider filled the water column at midshelf (Fig. 2E). The total duration of the resuspension event spanned more than one tidal cycle.

In contrast, the southward alongshore drift of the glider (Fig. 2B) in Hurricane Ivan in September 2004 indicated the storm center passed offshore. Hurricane Ivan tracked through the area on 18 September 2004 when the seasonal thermocline was still strong (Fig. 2D). Winds at the Delaware Bay buoy peaked at 16 m s^{-1} with waves at significant heights of 3.8 m and peak periods of 8 s. During Hurricane Ivan the glider was deeper, near 40–50 m. In this case, the sediment particles identified by the high backscatter were lifted to the base of the thermocline (Fig. 2F). Despite the intense mixing during the hurricane, the surface layer remained distinct from the bottom waters. The lack of response in the upper layer in the stratified season indicated that the backscatter events observed by the glider are most likely not bubbles that are being entrained from the surface as observed by Gargett et al. (2004) on the inner shelf. A similar mixing response within the lower water column only was observed for sediment resuspension on the outer shelf during Tropical Storm Ernesto, which also occurred when the shelf was still highly stratified (Bowers et al. unpubl.). Similar to the winter storms, the Hurricane Ivan resuspension event again occurred over a timescale longer than tidal.

Observed differences between the stratified and unstratified response to storm events in Fig. 2 prompted the following detailed study of a fall transition storm. The transition storm is expected to exhibit characteristics of both stratified and unstratified flows as the storm progresses. Data from the fall transition storm in 2003 were acquired by the first glider mission along the Tuckerton endurance line as shown in Fig. 3. The fall transect covers the time period from 28 October through 05 November 2003, with distance along-track measured from the starting point near LEO on the outbound leg. For the following discussion we consider 0–20 km from the LEO site as nearshore, 20–70 km offshore as midshelf, and 70–120 km as the outer shelf. Temperature and salinity data indicate that most of the midshelf region on 30 October and 01 November was well mixed. Inshore stratification on 28 October was very weak. Stratification on 02 November was present below about 40-m depth. The water was cold and salty, reflecting what remains of the summer cold pool. The glider also measured backscatter data along this same cross-section. Unlike temperature and salinity, the backscatter exhibited significant vertical variability and cross-shelf structure. Enhanced backscatter was observed nearshore, and in a bottom nepheloid layer out to the 65-m isobath. Low backscatter was found offshore and in the salty waters below the deep thermocline, suggesting a slopewater source. At about 30 km offshore of LEO, two short-lived resuspension events were observed which resulted in enhanced backscatter throughout the water column. The initiation of these events and their subsequent decay was rapid, on timescales less than 1 h (Fig. 3) and was correlated with a large fall transition storm.

A fall transition storm—The fall transition storm during this study was a classic "northeaster" event that occurred during late October and early November 2003. This storm began as a low pressure system that formed over North Carolina early on 29 October and rapidly propagated to the northeast, parallel to the coast. The center of the low pressure remained over land, passing New Jersey about midday on 29 October (Fig. 4A) when the barometric pressure dropped to 998 hPa. As the storm center continued its rapid movement into Maine on 30 October, the backside of this northeaster impacted the New Jersey shelf (Fig. 4B). The local wind records at the Tuckerton Meteorological Tower (Fig. 5) showed increasing winds initially from the southeast that then shifted direction with a strong burst of wind, approaching 10 m s^{-1}, from the northwest. In less than 6 h, the winds settled into a relatively steady period of westerlies for the next 12 h as barometric pressure climbed to 1025 hPa, and the sustained winds remained near 5 m s^{-1}. During this time significant wave heights at the Delaware Bay weather buoy (NOAA NDBC Buoy No. 44009) peaked at about 2 m on the evening of 29 October and decreased steadily on 30
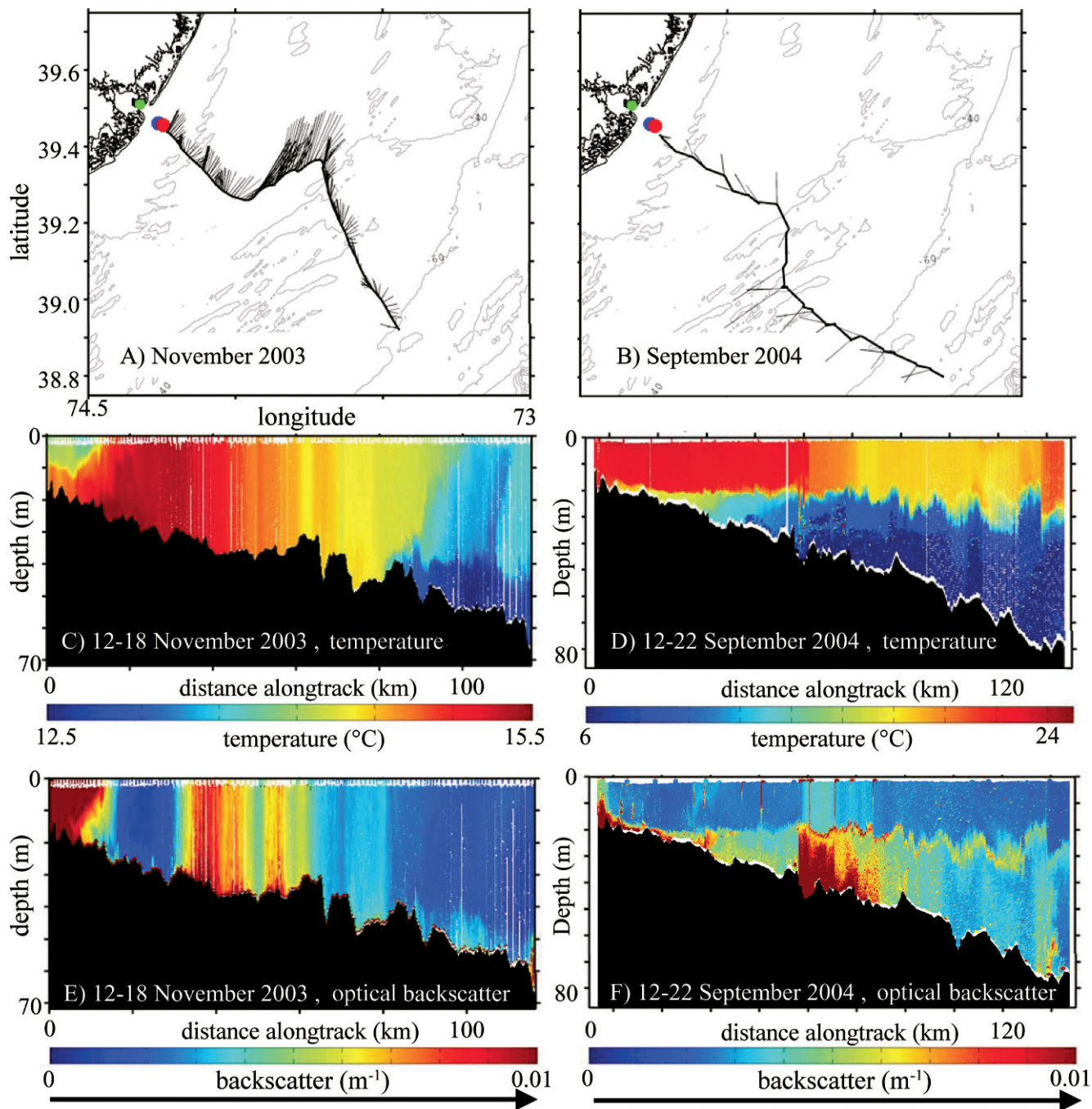
Fig. 2. Response to a winter northeaster (November 2003, left column) and a summer hurricane (September 2004, right column). (A, B) Glider tracks with vector stick plots showing the strong depth averaged storm currents forcing the glider alongshelf. Red and green circles as in Fig. 1. (C, D) Temperature pixels, and (E, F) backscatter pixels, are plotted as individual data points without interpolation. Arrows show direction of glider travel.

October to 1 m by the end of the day. Wave spectral peak periods ranged from 9 to 11 s.

Density, temperature, and salinity at the beginning of the storm were typical for fall conditions on the New Jersey Shelf (Fig. 6C, D, E). While the surface waters were slightly cooler than the bottom water, the water column was stably stratified due to the high salinity (32.7–32.9) near the bottom with a weak pycnocline at about 20 m below the surface. Below the pycnocline, backscatter values

(b_b470 nm) were three to four times higher than the surface waters. The weak water column stratification was eroded during the October 29th storm, transitioning to a fully mixed water column. Coincident with the erosion in stratification, there was a rapid increase in optical backscatter throughout the full water column at 0400 Greenwich mean time (GMT). By 0900 GMT, backscatter values declined with only a very thin layer of particles detected near the bed. This was followed with an abrupt
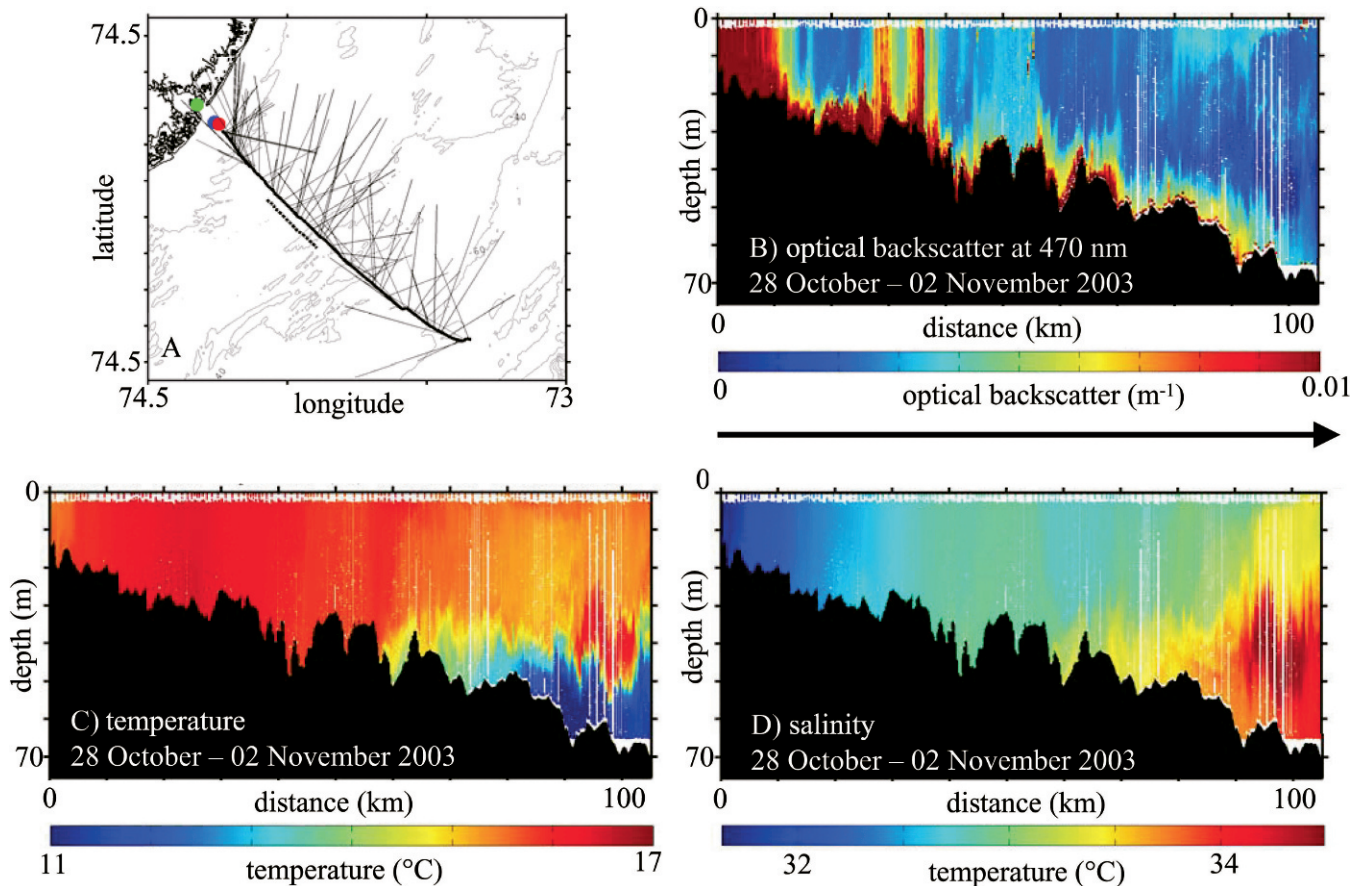
Fig. 3. The first cross-shelf Slocum glider transect on the Tuckerton endurance line, 28 October to 02 November 2003. (A) Track location and depth averaged current vector stick plot. The section of this transect plotted as a time series in Fig. 5 is indicated by the parallel dashed line. Red and green circles are the same as Fig. 1. (B) Backscatter at 470 nm, (C) temperature, and (D) salinity. Individual data points are plotted as color-coded pixels without interpolation. Arrow indicates the direction of glider travel.

change at 1000 GMT where the backscatter increased again for 2 h. The first full water column high backscatter event occurred over a seafloor that was sloping sharply up in the cross-shelf direction of the glider track, while the second occurred when the bottom was sloping slightly downward.

The portions of the water column associated with high values of b_b470 had low spectral backscatter ratios (Boss et al. 2004) (b_b470/b_b676, Fig. 6B) compared with the upper water column early in the event. In the high backscatter regions, the 20–30% range in the spectral ratio reflected a flattening in the backscatter spectrum. The relative shift in the material present in the water column was evident in the early periods of the storm when the backscatter ratio was lower in waters below the pycnocline and two to three times higher in the upper water column waters. When the pycnocline eroded and bottom material was injected into the surface waters, the backscatter ratio values dropped throughout the water column coincident with the enhanced backscatter. The variability in backscatter spectra also suggests that it would be difficult to convert the backscatter data to a particle concentration without information on the particle type and size distribution; however, we believe the threefold to fourfold increase in b_b during resuspension events does reflect changes in concentration. To minimize

the need for conversion to particle concentrations, subsequent analysis of backscatter data will be in terms of relative values within each profile. Profile to profile comparisons assume the bottom sediment is relatively uniform, a relatively safe assumption at midshelf in the MAB.

Geologic setting—During the last ice age of the Pleistocene, glaciers advanced as far south as Long Island. The MAB shelf remained south of the ice edge, was above sea level, and was covered with a network of river valleys dominated by the Hudson, Delaware, and Chesapeake Bay outflows. During the ensuing Holocene, sand and gravel deposited by the glacial meltwater streams was reworked by the rising Atlantic as the glaciers receded, leaving much of the MAB covered with a layer of sandy sediments. The spatial distribution of bottom sediment types in the MAB was summarized by Amato (1994) using data mostly from U.S. Geological Survey databases or state geological surveys and compiled for oil and gas lease sales. The main feature of the MAB sediment distribution is the nearly shelf-wide alongshelf band of greater than 75% medium (0.025–0.05 cm) to coarse (0.05–0.2 cm) grained quartz sand with an average thickness of 5 m. A narrow band of mixed medium to fine sand and silt covers the shelf break,
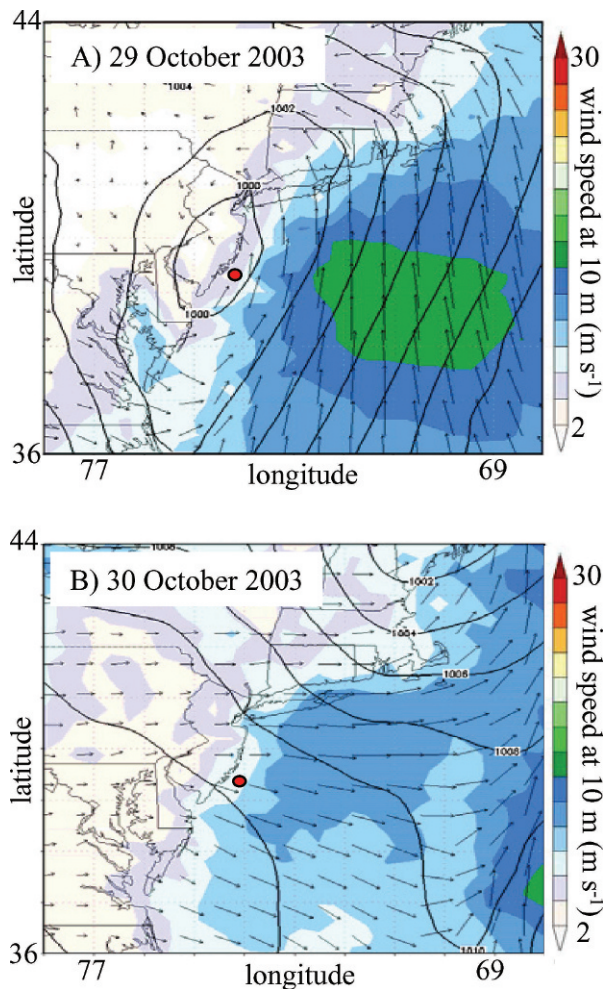
Fig. 4. Weather research and forecast model wind and sea level pressure forecasts for the October 2003 northeaster. (A) 1200 GMT on 29 October 2003, and (B) 0000 GMT on 30 October 2003. Pressure is in hPa, wind speed in m s^{-1}.

with deepwater sediments further offshore consisting of greater than 75% clay. The most notable large-scale exception to this alongshore banding is the large mud patch that occurs south of Martha's Vineyard and extends from midshelf to the shelf break. Most of the New Jersey shelf is in the medium sand grain size range. Mixtures of medium to fine sand and silt are found in a narrow (about 10-km wide) band along the coast, and in a narrow (again about 10-km wide) cross-shelf band extending from New York Harbor to the southeast along the Hudson Shelf Valley. Just south of the Hudson Shelf Valley are parallel elongated bands of gravelly sand associated with old meanders of the Hudson River (Schlee 1964). Focusing further on the shelf off southern New Jersey in the vicinity of the endurance line, fine-scale variability in the nearshore mixed sediments associated with the small shore-oblique sand ridges has been noted (Twitchell and Able 1993). But once beyond this narrow nearshore band, the entire cross-shelf section to the shelf break is dominated by the medium quartz sands overlaying the larger scale shore-parallel ridges often found at midshelf (Duane and Stubblefield 1988).

A series of wave–current–sediment interaction studies in this region (Styles and Glenn 2005) characterized the mean sediment grain size diameter on this sandy shelf as 0.04 cm. The still water fall velocity of this size sediment grain is approximately 5.6 cm s^{-1}. The backscatter record from 1400 GMT (Fig. 6A) captures the transition from high backscatter throughout the water column (profiles 1 and 2) to low backscatter nearly to the bottom (profile 3). With six profiles in this hourly record, the time between profiles is approximately 10 min. If the backscatter was caused by resuspended bed sediment that then falls out of suspension after the forcing subsides, the sediment would have to fall a distance of approximately 30 m in 10 to 20 min, resulting in an estimate of the fall velocity between 5 cm s^{-1} and 2.5 cm s^{-1}. This estimate is consistent with the type of sediment that is widely available on the sandy MAB shelf (Amato 1994) and suggests that the storm resuspended the sediment from the sandy bottom.

Physical processes driving the sediment resuspension— Several factors can impact the resuspension and transport of sediment. These factors include storm-driven currents, waves, tides, bottom topography, and Langmuir circulation.

The importance of the surface waves in driving the backscatter variability was examined and appeared not to be the major mechanism driving the variability observed in the resuspended sediment. Waves spectral parameters (Fig. 7) were calculated from the bottom pressure sensor at the LEO cabled observatory using the methods of Tucker and Pitt (2001). The distance between the LEO cable node and the glider was smaller than the synoptic scale of the storm winds (tens of kilometers compared with hundreds kilometers), especially during the westerly winds on the back-end of the storm. Wave heights, when atmospheric pressure was rising, decreased from 1.3 m to 0.7 m at a relatively steady rate. During that period the wave spectral peak periods increased. Similar observations from the NOAA weather buoy off of Delaware Bay (Fig. 5) indicated that the surface wave response was at the spatial scale of the storm. The larger wave heights early in the storm and the relatively steady peak periods produced large bottom orbital velocities that peaked at about 20 cm s^{-1} and decayed to about 15 cm s^{-1}. With the methodology of Glenn and Grant (1987), bottom orbital velocities of this magnitude result in a Shields parameter that exceeds the initiation of motion criteria for the sediments in this region by about an order of magnitude (Traykovski 2007). Although the waves are capable of mobilizing the bed sediment throughout this event, the highest bottom orbital velocities occurred earlier in the storm when the sediment was only suspended 10 m to the base of the pycnocline. The decrease in wave forcing was not expected if wave induced resuspension and wave-enhanced vertical mixing was the primary driver of the variability in the sediment resuspension near the end of the storm on 30 October. Because the angle between the currents and waves does not have a strong influence on the magnitude of the total boundary shear stress, slowly decreasing wave bottom orbital velocities, combined with the relatively steady current
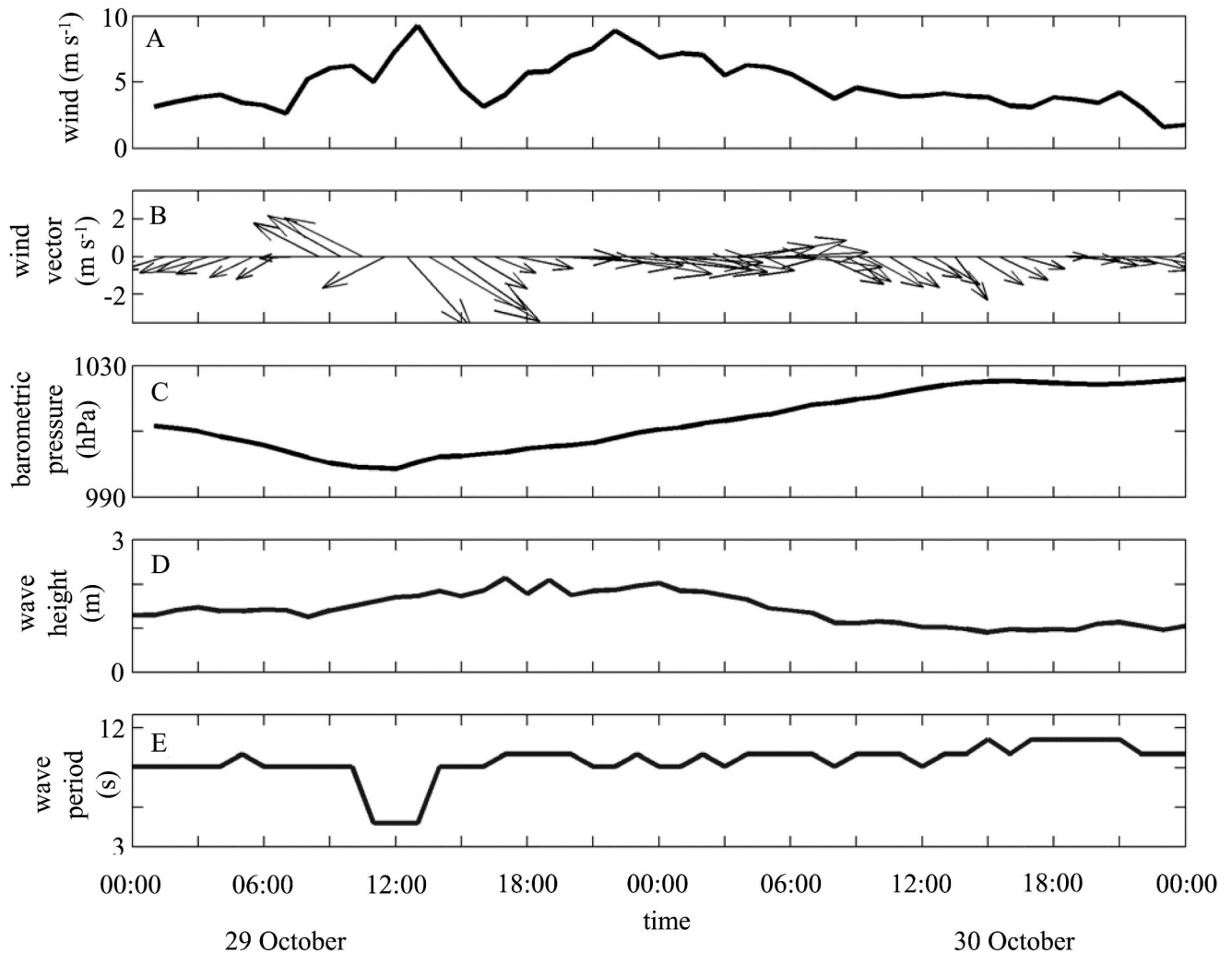
Fig. 5. Observed wind and wave data during and after the passage of the 29–30 October 2003 northeaster. (A) Wind speed, (B) wind vector (m s^{-1}), and (C) barometric sea level pressure from the Tuckerton Meteorological Tower. (D) Wave height and (E) peak wave period from the Delaware Bay weather buoy.

magnitudes discussed below, should, in theory, produce a relatively steady sediment resuspension profile in the water column.

As wave forcing was unlikely the primary driver for the sediment resuspension, the average vertical velocity of the glider was calculated for each profile during the storm (Fig. 7D). The values averaged 14.5 cm s^{-1} with a standard deviation of 1 cm s^{-1}, and no noticeable trend over the record. Full water column Langmuir cells measured by Gargett et al. (2004) using a fixed current meter had vertical limbs that alternated between positive and negative vertical velocities about every 10 to 20 min. With cross-wind currents typically near 7 cm s^{-1}, they estimated the horizontal scale of the cells as 40 m to 70 m. The magnitude of the alternating upward and downward velocities matched the expected 0.008 times the wind speed rule used by Gargett et al. (2004), producing a total vertical velocity difference exceeding 10 cm s^{-1} during the storm. During this study, the wind speed of $\geq$5 m s^{-1} resulted in an estimate of the velocity difference between the vertical limbs of potential Langmuir cells as $\geq$8 cm s^{-1}. The

relatively steady glider vertical velocity of about 15 cm s^{-1} covers a typical 30-m surface-to-bottom profile in about 200 s. During this sampling interval, the glider is moving at typical horizontal speeds of 30 cm s^{-1}, covering a horizontal distance of about 60 m relative to the water. The horizontal scale of the glider sampling relative to the water is thus similar to the horizontal scale of the Langmuir cell limbs observed by Gargett et al. (2004). The time series in Fig. 7D indicated there were no significant changes in the glider vertical velocities over time, and the full water column variations in optical backscatter occurred over longer timescales than that of individual profiles. Since both the glider and the potential Langmuir cells are advected by the same mean currents, the expected backscatter response for a glider crossing a Langmuir cell depends on the crossing angle associated with the glider's velocity relative to the water. For shallow crossing angles, we would expect variations on the scale of a few profiles, with variations in vertical velocity correlated with variations in the backscatter. For steep crossing angles, we would expect banding between low backscatter and high
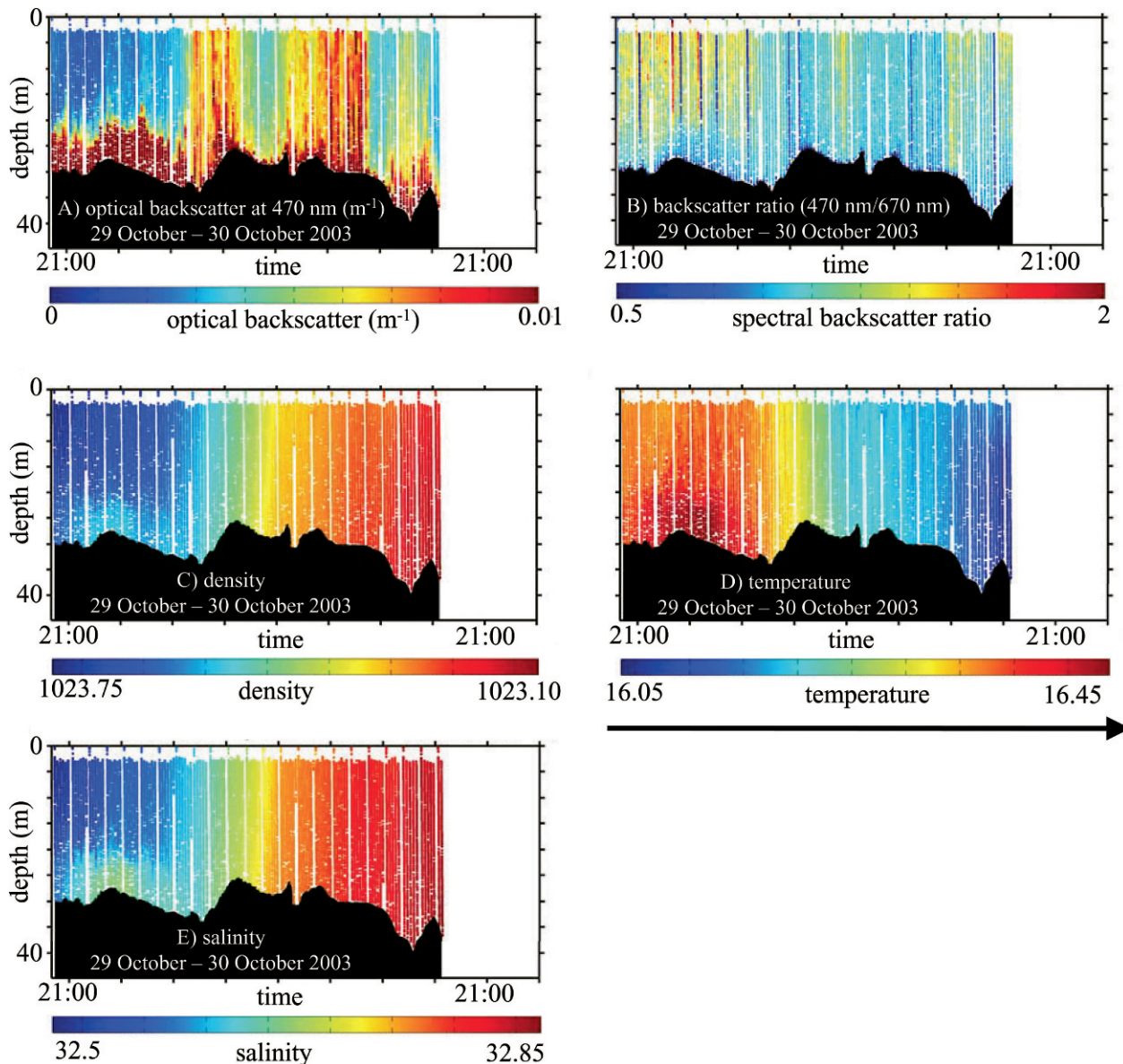
Fig. 6. Time series of profiles collected by the glider during 29–30 October 2003 northeaster in the location indicated by the dashed line in Fig. 3. (A) Backscatter at 470 nm, (B) ratio of the backscatters at 470 nm and 676 nm, (C) density, (D) temperature, and (E) salinity. Data points are again plotted as pixels without interpolation. Arrow indicates direction of glider travel.

backscatter regions within a profile as the glider quickly crosses between upward limbs and downward limbs. Neither of these features in the detailed velocity or backscatter observations was observed. As noted by Gargett et al. (2004), the fall transition storm they observed on the inner shelf did not exhibit evidence of Langmuir circulation even though particles were suspended throughout the full water column. The fall transition observed here also was forced by winds from the west, resulting in a reduced fetch for the breaking surface waves required for the Langmuir cells and the least likely wind direction to produce cells that reach the bottom (A. Gargett pers. comm.). We therefore conclude that while the end result of a full water column resuspension event is consistent with the expected impact of full water column Langmuir

circulation cells, we cannot find evidence to support that conclusion in this storm.

Another mechanism potentially driving the resuspension of sediment is the interaction between the winds and currents (Fig. 8). Winds from the Tuckerton Meteorological Tower were averaged for 1-h intervals to match the glider's observed hourly average of the depth average currents. On 29 and 30 October, the wind speed steadily decreased from 9 m s^{-1} to about 2 m s^{-1} (Fig. 8A).

The average current speed runs about 20 cm s^{-1}, with local peaks near 25 cm s^{-1} at 0300 GMT and 30 cm s^{-1} at 1600 GMT. A local minimum is found near 1000 GMT coincident in time with the low backscatter observed in Fig. 8E. The wind vector (Fig. 8C) is relatively steady in direction, with only a slight shift from west to northwest
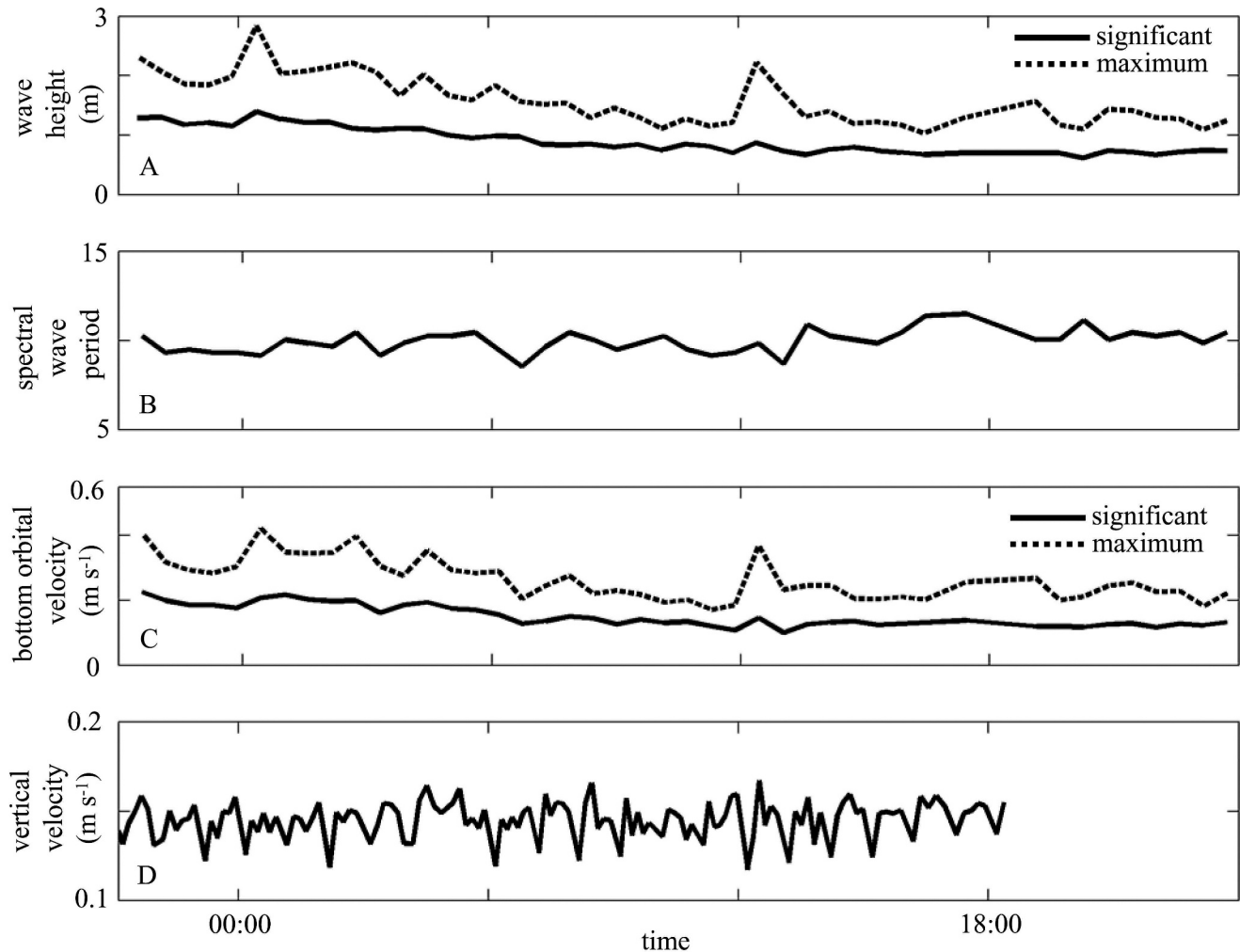
Fig. 7. Time series plots of potential sediment resuspension forcing starting late 29 to 30 October 2003. (A) Significant wave height (solid) and maximum wave height (dashed) and (B) spectral peak wave period at the Long-term Ecosystem Observatory, (C) significant wave bottom orbital velocity (solid) and maximum wave bottom orbital velocity (dashed) that the observed waves would generate in the 30-m water depth of the glider, and (D) the average vertical velocity for each downcast observed by the glider.

about 0600 GMT and back again about 1700 GMT. In contrast, current directions are much more variable. To determine the nature of that variability, the M2 tidal constituent was extracted from the current data and is plotted in Fig. 8D along with the residual. The detided residual, like the wind, is remarkably steady in direction, flowing primarily in the alongshore direction, often 60 to 90 degrees to the left of the wind. The leftward turning of the currents relative to the wind result is similar to the unstratified seasonal average found by Kohut et al. (2004) on the inner shelf, and also during the passage of Hurricane Floyd (Kohut et al. 2006). Hurricane Floyd followed nearly the same storm track as this northeaster, and as it passed the New Jersey shelf, currents throughout the water column observed by HF radar and acoustic Doppler current profilers were found to be about 60–90 degrees to the left of the wind direction. It appears that similar processes that result in the leftward turning of the current vector are consistent with the dynamics of the bottom boundary layer active at midshelf in the unstratified season.

Finally we examine the tidal component of the depth averaged current plotted in Fig. 8D. Maximum tidal velocities were slightly less than the residual and tended to flow in the across-shore direction. The peak in the offshore tidal flow occurred at 0900 GMT and corresponded exactly with the observed drop in optical backscatter in the water column. As soon as the tidal velocities reversed, and the tidal flow was again toward the coast, the optical backscatter again increased throughout the water column. Thus it appears that the observed variations in the full water column events are associated with an interaction with the tides.

This raises the question: What type of interaction is being observed? If the observed changes in optical backscatter were associated with advection, we would have expected to see the exact opposite behavior from that encountered here. Since more sediment is suspended nearshore as wave bottom orbital velocities increase, an offshore flow would be expected to increase backscatter while an onshore flow would be expected to cause a
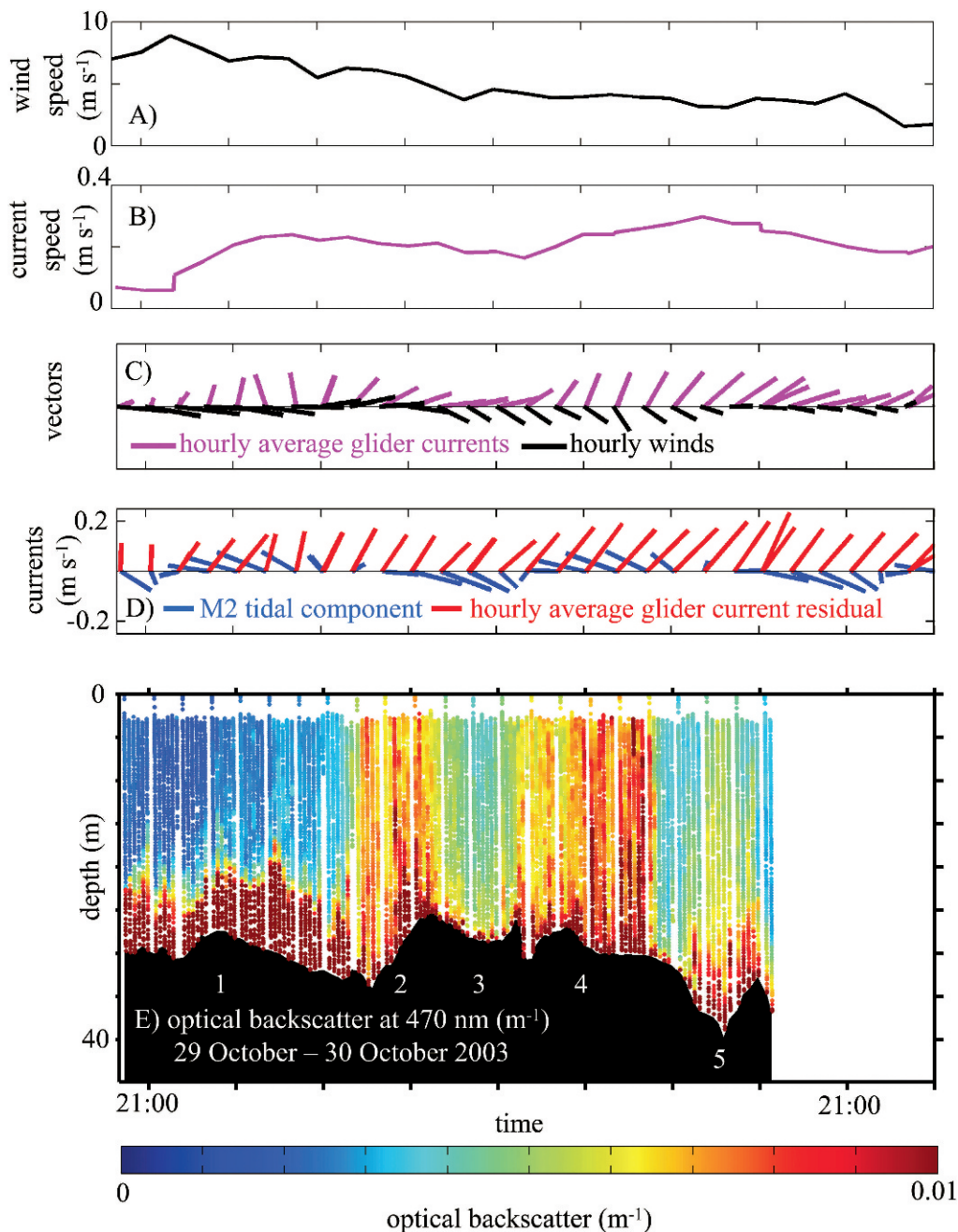
Fig. 8. Time series plots of potential sediment resuspension forcing starting late 29 to 30 October 2003. Plotted are (A) hourly averaged wind speed from the Tuckerton meteorological tower (black), (B) hourly averages of the depth averaged current speed calculated from the glider drift (magenta), (C) hourly depth averaged vector currents from the glider (magenta) and hourly averaged vector winds (black) from the Tuckerton meteorological tower, (D) the M2 tidal component (blue) and the residual (red) from the hourly depth averaged glider currents, (E) backscatter at 470 nm observed by the glider. Numbers 1–5 indicate five different sampling regimes discussed in the text.

decrease. The timing of the observed variability in the backscatter, however, is consistent with resuspension processes if the nonlinear interactions of waves, tides, and currents similar to the modeling results of Keen and Glenn (1995) are considered. The geometry of the tides and residual flows is such that they enhanced the total flow during the high optical backscatter events and reduced the total flow during the low backscatter events. Because the sediment resuspension process is nonlinear, the differences

in flow regimes were amplified. It therefore appears that understanding the full backscatter history of this storm must take into account the interaction of the surface and bottom boundary layers as the stratification erodes and the nonlinear interactions of the relatively steady alongshore residual current, the oscillatory tides, and the steadily decreasing wave bottom orbital velocities.

The time-varying effect of these processes on turbulent mixing was investigated using the backscatter profiles

acquired by the glider. Assuming the particles are of a similar size class, optical backscatter intensity would be expected to be roughly proportional to sediment concentration. Based on the backscatter profiles, five time periods can be highlighted in Fig. 8E. The first time period corresponds to still stratified conditions near the storm peak. Backscatter profiles during this time period indicate that significantly larger sediment concentrations are expected in the bottom layer below the eroding pycnocline, but they then decay rapidly with increasing distance from the bed. The final four time periods occur after the transition to unstratified conditions. These time periods are characterized by alternating full water column bands of high and low backscatter. Compared with the first time period, sediment concentrations near the bed are slightly lower during the unstratified times, but there is little decay with distance from the bed.

Comparison with theory—Theory for describing suspended sediment concentration profiles in combined waves and currents is well developed (Glenn and Grant 1987; Styles and Glenn 2000). Above the wave boundary layer, an assumed Fickian diffusion in the absence of self-stratification results in a standard Rouse profile

$$C(z) = C(z_r)[z / z_r]^{[-\gamma w_f / \kappa u_*]} \quad (1)$$

where $C(z)$ is the concentration profile that varies with the vertical coordinate z, $C(z_r)$ is the concentration at the arbitrary reference height z_r, w_f is the particle fall velocity, u_* is the turbulent shear velocity, γ is the assumed constant ratio between the unstratified eddy diffusivities of momentum to mass, and κ is von Karman's constant. In the Fickian model, u_* represents the tendency of turbulent diffusion to suspend sediment in the water column, and w_f represents the tendency for the sediment to fall out of suspension. The ratio of w_f to u_* controls the slope of the concentration profile. If this ratio is small $(w_f \ll u_*)$, there is significant turbulent mixing, and very little decay of the sediment concentration as a function of distance from the bed.

The Rouse concentration profile in Eq. 1 plots as a straight line on log–log paper. Normalizing the concentration profile by the concentration at the reference height z_r and taking the natural logarithm gives the following solution for the fall velocity to shear velocity ratio

$$wf / u_* = -(\kappa / \gamma)(\ln[C(z) / C(z_r)] / \ln[z / z_r]) \quad (2)$$

The constant $\kappa = 0.4$ is well known, while quoted values for γ typically range between 0.74 and 1 (Glenn and Grant 1987). Assuming a value of $\gamma = 0.8$ gives a very simple equation for the w_f/u_* ratio, namely, it is negative half of the slope (assuming z is the independent variable on the log–log plot).

To develop estimates of the w_f/u_* ratio from the glider data, we assume, as suggested by the backscatter ratio (b_b470/b_b676) in Fig. 6B, that similar grain sizes dominate the resuspended material below the pycnocline during time period 1 and throughout the water column in time periods 2–5 of Fig. 8E. Similar size sediment grains leads to a second assumption that the observed backscatter is approximately proportional to the sediment concentration. With these simplifying assumptions in mind, the glider backscatter profiles were transformed into a coordinate system measured positive upward from the seabed and time averaged within each sampling interval to produce a time series of hourly profiles. The arbitrary reference height z_r was chosen as 1.5 m above the seafloor, a point close to the bottom inflection point of the glider's sawtooth trajectory. Choosing a reference height even closer to the bed would affect the time average, with fewer and fewer points available as the glider typically completed its inflection and turned back toward the surface just below this level. The time average backscatter profile is then normalized by the observed backscatter at the reference height of 1.5 m for each hourly segment. Using the normalized backscatter profiles as a proxy for the normalized sediment concentration profiles, we plot the natural logarithm of the normalized backscatter as a function of the natural logarithm of the normalized height above the seabed (Fig. 9). For each of these 20 hourly profiles distributed across the storm resuspension event, the hourly average density profile is also plotted on the same vertical scale.

Density profiles in Fig. 9A–F show how the weakened summer pycnocline is eroded during this mixing storm. Initially (Fig. 9A), the bottom of the pycnocline is found near a height of ln $(z/z_r) = 1$, which in physical space corresponds to a height of 4 m above the bed. Density in the well-mixed bottom layer begins the time series near a value of $\sigma = 23.87$. Over time, the height of the well-mixed bottom boundary layer grows, causing the bottom of the pycnocline to move upward, away from the bed until the full water column is well mixed (Fig. 9G) at a density similar to the initial bottom boundary layer. For the next 10 h, the water column remains well mixed while the density steadily increases. Near the end of the event (Fig. 9R–T), the stratification slowly builds in the upper portion of the water column.

The time history of the normalized backscatter profiles is clearly linked to the evolving density structure. In the well-mixed bottom boundary layer, consistent with the theoretical structure implied by the Rouse profile, the relative backscatter profiles decay along a straight line when plotted on this log–log scale until the bottom of the pycnocline is reached. At that point, even the small amount of stratification caused by the temperature and salinity structure appears to be enough to inhibit the vertical turbulent flux of sediment and significantly limit the amount of resuspended material reaching the upper water column. As the storm progresses and the bottom of the pycnocline moves upward so does the region in which the relative backscatter profiles exhibit the straight line Rouse-like behavior. By Fig. 9G and beyond, the pycnocline is gone, and the normalized backscatter profiles are Rouse-like over the full water column.

To calculate the slope of each normalized backscatter profile in the bottom boundary layer, a straight line was fit to the normalized backscatter values below the pycnocline in Fig. 9A–F, and for the full water column for the remainder. R^2 values for the fit during the initial stratified
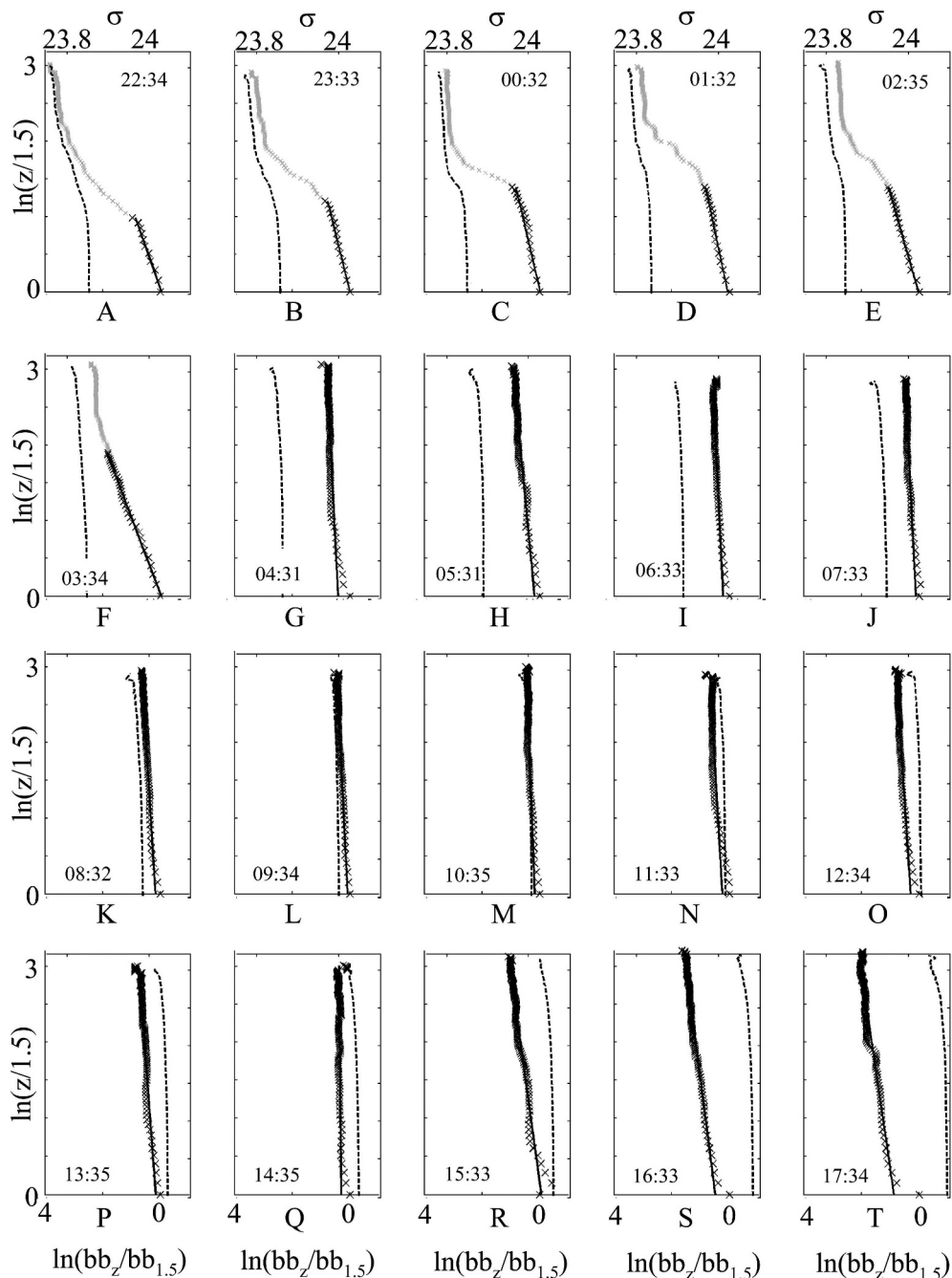
Fig. 9. Profiles of density profiles (dashed line, top scale) and logarithm of the normalized backscatter (bottom scale) plotted vs. the logarithm of the normalized height above the bed. Normalized backscatter values used in each of the linear fits are plotted in bold, along with the best fit straight line (solid). Normalized backscatter values not used in the fit are plotted as gray.

period range from 0.94 to 0.99 and average 0.98. During the full water column resuspension events, however, the best fit line is nearly vertical. When comparing the vertical lines with the data points, the fits appear to be of similar quality as earlier in the storm. The resulting R^2 statistic, however, no longer adequately characterizes the quality of a nearly vertical line fit, so a different statistic is needed. We therefore adopted the root mean square (RMS) difference between the best fit line and the actual points and track this value across the full time series (Fig. 10A). The natural log of the relative concentration typically varies between 0 and -3 for each of the 20 profiles, with RMS differences of the fit two orders of magnitude lower, averaging 0.05 and ranging from 0.02 to 0.11 over the interval. Based on the slope of the best fit straight lines, the resulting w_f/u_* ratio is plotted in Fig. 10B. Early in the storm when the water column was stratified, the velocity ratio is similar to what would be expected for wave-current induced sediment
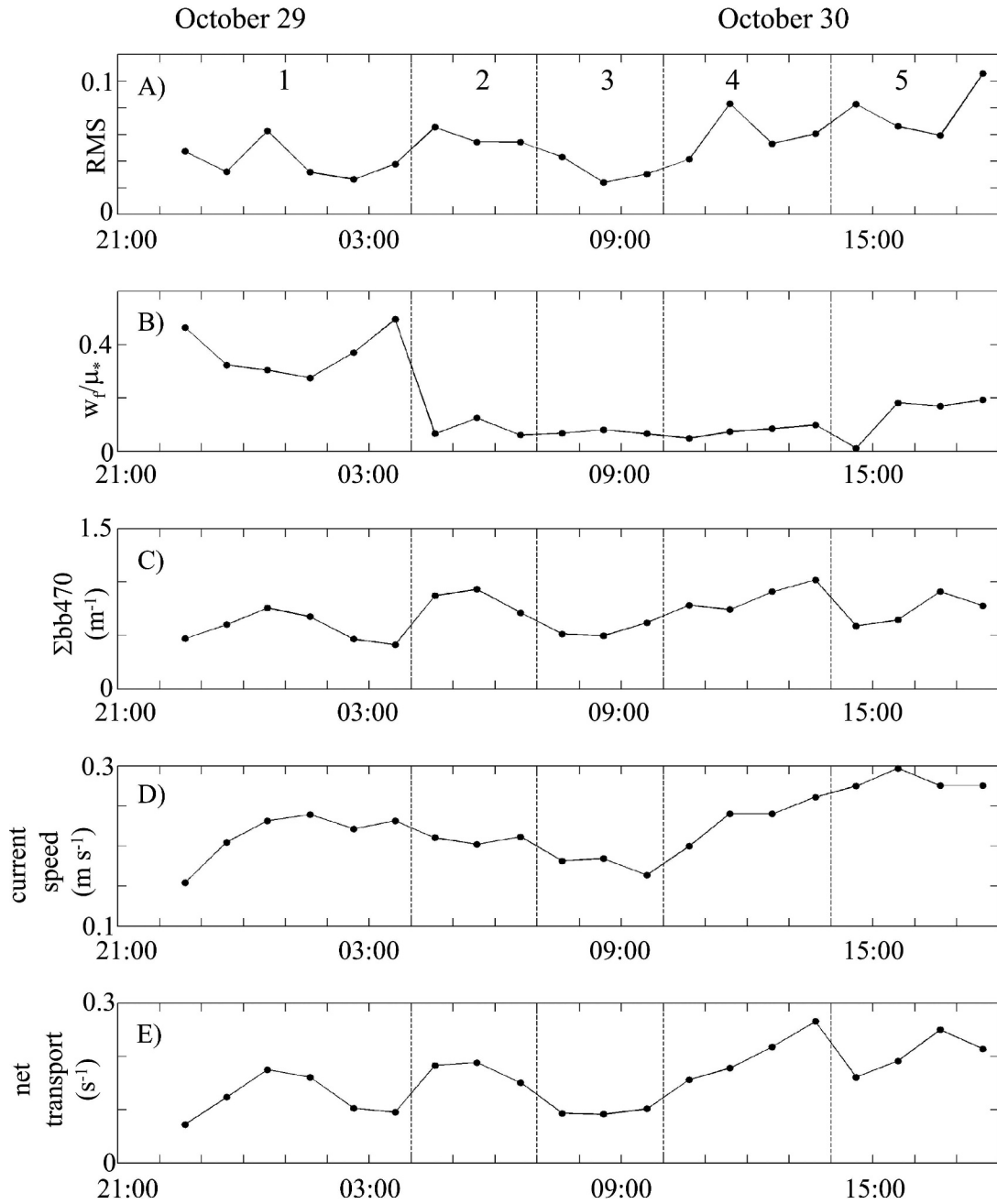
Fig. 10. Time series derived from each of the hourly profiles in Fig. 9. (A) RMS difference between the linear fit and the observed normalized backscatter, (B) ratio of the fall velocity to the friction velocity, (C) vertically integrated backscatter, (D) depth average current speed from the glider, and (E) net transport estimated by multiplying vertically integrated backscatter by the current speed. Numbers 1–5 correspond to the same time periods labeled in Fig. 8.

resuspension in shallow water during a storm. After the stratification is lost, the ratio drops by nearly an order of magnitude. If wave-current interaction was the only mechanism for enhanced turbulent mixing in the water column, this would imply that the combined wave and current bottom stress was significantly increasing while the currents are steady and the wave bottom orbital velocities were dropping. While there may be a drop in the fall velocity during this time period to partially compensate for the lower ratio, an order of magnitude drop in fall velocity

would require a similar scale drop in grain size. Optical data does not support this based on changes in the absolute values and spectral backscatter ratios. The final possibility is the interaction with the turbulence in the wind-driven surface layer with the wave-enhanced bottom boundary layer; however, observations of this type of interaction are sparse.

Potential sediment transport during the storm—To determine the potential effect on sediment resuspension

and transport, the total integrated backscatter was calculated for each profile, and the integrated backscatter was multiplied by the depth average current, the only water column current observation available from the glider, to estimate the associated transport (Fig. 10C–E). During the early part of the storm when the water column was stratified and the high sediment concentrations were confined to the lower layer, using the full depth averaged current would likely overestimate the transport. Three peaks in the estimated total load of resuspended sediment were observed, all of similar magnitude. The lowest of the three peaks was the first, occurring during the early stratified portion of the event when surface waves were the highest. Even though near bottom sediment concentrations were lower during the peak load time periods after the stratification was eliminated, the full water column appears to be capable of supporting a larger total amount of sediment in suspension. In contrast to the total suspended load estimates, the time series of depth averaged current speeds inferred from the glider has two broad peaks, with the low speeds observed between 0700 and 1000 associated with the time-varying tidal currents opposing the relatively steady storm-driven flows. This period of low currents corresponds to a time period of low integrated backscatter. Transport estimates have a similar pattern to the sediment load, with three peaks during the storm event. The high sediment load and strong current speeds result in the greatest transport occurring over 12 h after the waves started decreasing. During this decay phase of the waves after the stratification is lost, the highest transport occurs in a pair of short 3- to 4-h duration hops. This example illustrates that the greatest sediment transport is not necessarily tied to the peak of the storm, and that the total history of the storm, which likely spans a cycle or two of the tide, must be considered when examining sediment transport patterns on this shelf.

Discussion

Optical data sets from the glider transects have been examined (Glenn et al. 2004*a*) and used to identify at least three cross-shelf regimes for sediment transport on the MAB shelf: (1) the inner shelf with persistently high optical backscatter and a seasonal pycnocline that can be present or absent depending on the history of upwelling or downwelling favorable winds, (2) the midshelf where a persistent seasonal stratification limits the direct linkages between the upper wind-driven boundary layer and the lower combined wave and current boundary layer until a fall transition storm mixes the full water column, and (3) the outer shelf where the depths limit the effect of surface waves to only the most severe storms. Most previous sediment transport studies on the New Jersey shelf are focused either on the ridge and swale topography of the inner shelf, or on the Hudson Shelf Valley (Harris et al. 2003), and all use traditional bottom tripods with fixed instruments. The ability to use inexpensive mobile profiling glider platforms opens up much larger regions for future long-term study.

In the relatively unexplored sediment transport regime of the midshelf of the MAB, glider observations have provided new challenges for coupled physical-sediment transport models. Detailed analysis of the mixing storm revealed that even a small amount of stratification appeared to restrict mixing of sediment across the weakened summer pycnocline. Mixing of the full water column did not occur during the peak winds and waves but did occur later in the storm as the bottom boundary layer grew to fill the water column. Tides and surface waves appeared to enhance turbulent fluxes that mixed sediment throughout the water column once the stratification was eroded. Consistent with the type of bottom sediment available in this midshelf region, these particles rapidly dropped out of suspension whenever the combined current, tide, and wave forcing declined. Other reasons for the observed variability were ruled out. Bottom sediments at midshelf in the vicinity of the Tuckerton endurance line are relatively uniform. One full water column resuspension event occurred on the onshore side of a midshelf ridge, the other on the offshore side. Mean currents estimated from the glider drift also indicated that the changes in the vertical distribution of suspended sediment were not associated with changes in the advection directions. Sediment resuspension and transport peaks were not tied to the peak in the wave bottom orbital velocities, lacked evidence for full water column Langmuir cell activity, and appeared to be more correlated with the interactions between relatively steady storm currents, tides, and declining waves rather than the topographic variations in space. This indicated the potential for nonlinear coupling between the three flow components, a new field result consistent with previous modeling studies of the New Jersey shelf.

A significant advance developed here is the use of profiling optical sensors on mobile platforms to provide quantitative estimates of the shape of sediment resuspension profiles. The shape of the normalized time-averaged backscatter profiles is consistent with the theoretical shape derived from the conservation of sediment mass equation using standard closure techniques, namely, that the sediment concentration is expected to decay with distance from the bed along a line of constant slope on a log–log plot. The observation that the slope of this line changes significantly as soon as the stratification is eroded but the backscatter ratio at two frequencies does not has significant implications for the role of turbulent mixing. It implies that once the bottom boundary layer grows to fill the water column, the characteristic turbulent velocity scale increases, possibly due to the now unhindered interaction of surface and bottom boundary layers. The dominance of a bottom boundary layer response of the water column during a strong tropical storm forcing event on the inner shelf of New Jersey was similarly noted by Kohut et al. (2006).

Future advances—The ability to average subsequent optical backscatter profiles sampled by a single profiling sensor and return mean profiles with shapes consistent with theory opens up new possibilities for future sediment transport studies. The new perspective is similar to the first near bottom current profiles returned from the Coastal Ocean Dynamics Experiment (CODE) (Grant et al. 1984),

where the log profiles acquired in the bottom boundary layer with new acoustic current meter technologies provided clear evidence of wave-current interaction and prompted years of research using similar sensors mounted on tripods. The subsequent and still continuing observations of near bottom current and sediment concentration profiles using both acoustic and optical sensors mounted on tripods, some attached to cabled seafloor observatories, prompted further refinements of the theoretical models for the current and suspended sediment profiles in the near bed constant stress layer. These advanced bottom boundary layer models have been coupled to three-dimensional physical circulation models through community based efforts (Sherwood et al. 2000), but validation data sets of observed sediment responses for three-dimensional models are few. While many acoustic sensors can acquire water column profiles, optical, temperature, and salinity sensors collect point measurements and thus require either multiple cross-calibrated sensors maintained in a vertical array or single sensors that must be profiled through the water column. Profiles of suspended sediment are required to evaluate the observed gradients in the sediment mass conservation equation used in theoretical models. But multiple cross-calibrated sensors are expensive to acquire and logistically difficult to operate, especially considering the resolution required to resolve the vertical gradients often observed at meter or finer length scales. Fixed autonomous profilers can potentially cycle a suite of sensors through the water column, but few autonomous profilers have proved their durability. Cabled observatories allow for point profiling; however, they fix the location of the studies to the installed node locations. Autonomous underwater gliders are emerging as a transformational tool for sediment transport scientists that will extend data collection beyond fixed platform locations. The gliders have already demonstrated they can be synergistic with traditional sediment transport studies from fixed platforms, providing a spatial perspective not readily available from a single point. Key to the gliders' success is their ability to carry flexible sensor payloads, their ability to remain deployed for long time periods compared with the length of a storm, and their potential for conducting adaptive sampling experiments.

These observations provide a framework for designing future experiments to study sediment transport to improve theoretical models. In the MAB, deploying gliders with optical sensors into all three cross-shelf regions simultaneously to collect storm data during both the stratified and unstratified time periods is possible since gliders are relatively inexpensive. Distributed arrays of optical gliders also could be used to study the role of advective processes. Turbulence sensors that are just now being deployed on gliders will enable observations of the details of the mixing profiles to help resolve questions of coupling between surface and bottom boundary layers. The combination of traditional and new sensors will help answer questions on the mixing processes responsible for the vertical profiles of suspended sediment, the timing of sediment loads relative to the wave, Langmuir cell, tide, and storm current forcing, and the variations in sediment loads in space in relation to topographic features or fronts. Ultimately this will provide guidance on which processes need to be included in bottom boundary layer and sediment transport models. Model sensitivities will in turn provide guidance on which processes need to be further sampled and studied. The ability to rapidly adjust glider sampling schemes makes them an attractive interactive platform for future storm studies.

References

AMATO, R. V. 1994. Sand and gravel maps of the Atlantic continental shelf with explanatory text., U.S. Department of Interior, Minerals Management Service, OCS Monograph, MMS 93-0037. 35 p.

BABIN, S. M., J. A. CARTON, T. D. DICKEY, AND J. D. WIGGERT. 2004. Satellite evidence of hurricane-induced plankton blooms in the ocean desert. J. Geophys. Res. **109:** C03043, doi:1029/2003JC001938.

BEARDSLEY, R. C., AND W. C. BOICOURT. 1981. On estuarine and continental shelf circulation in the Middle Atlantic Bight, p. 198–233. *In* B. A. Warren and C. Wunsch [eds.], Evolution of physical oceanography. MIT Press.

BISCAYNE, P. E., C. N. FLAGG, AND P. G. FALKOWSKI. 1994. The shelf edge exchange processes experiment, SEEP-II: An introduction to hypotheses, results and conclusions. Deep-Sea Res. **41:** 231–253.

BOSS, E., W. S. PEGAU, M. LEE, M. S. TWARDOWSKI, E. SHYBANOV, G. KOROTAEV, AND F. BARATANGE. 2004. The particulate backscattering ratio at LEO 15 and its use to study particles composition and distribution. J. Geophys. Res. **109:** C01014, doi:10.1029/2002JC001514.

CASTELAO, R. M., S. GLENN, O. SCHOFIELD, R. CHANT, AND J. KOHUT. 2008. Seasonal evolution of hydrographic fields in the central Middle Atlantic Bight from glider observations. Geophys. Res. Lett. **35:** L03617, doi: 10.1029/2007GL032335.

CHANG, G. C., T. D. DICKEY, AND A. J. WILLIAMS III. 2001. Sediment resuspension on the Middle Atlantic Bight continental shelf during Hurricanes Edouard and Hortense: September 1996. J. Geophys. Res. **106:** 9517–9531.

COLLE, B. A. 2003. Numerical simulations of the extratropical transition of Floyd (1999): Structural evolution and responsible mechanisms for the heavy rainfall over the Northeast United States. Mon. Weather Rev. **131:** 2905–2926.

DAVIS, R. E., C. E. ERIKSEN, AND C. P. JONES. 2003. Technology and applications of autonomous underwater vehicles, p. 37–58. *In* G. Griffiths [ed.], Autonomous buoyancy driven underwater gliders. Taylor & Francis.

DUANE, D. B., AND W. L. STUBBLEFIELD. 1988. Sand and gravel resources: U.S. Atlantic continental shelf. *In* R. E. Sheridan and J. A. Grow [eds.], The geology of North America, the Atlantic continental margin. U.S. Geological Society of America, **1–2:** 481–500.

EVANS, J. L., AND R. E. HART. 2003. Objective indicators of the life cycle of extratropical transition for Atlantic tropical cyclones. Mon. Weather Rev. **131:** 909–925.

GARGETT, A., J. WELLS, A. E. TEJADA-MARTINEZ, AND C. E. GROSCH. 2004. Langmuir supercells: A dominant mechanism for sediment resuspension and transport in shallow seas. Science **306:** 1925–1928.

GLENN, S. M., W. BOICOURT, B. PARKER, AND T. D. DICKEY. 2000. Operational observation networks for ports, a large estuary and an open shelf. Oceanography **13:** 12–23.

———, AND W. D. GRANT. 1987. A suspended sediment stratification correction for combined wave and current flows. J. Geophys. Res. **92:** 8244–8264.

———, AND O. SCHOFIELD. 2004. Observing the oceans from the COOLroom: Our history, experience, and opinions. Oceanography 16: 37–52.

———, AND OTHERS. 2004a. The expanding role of ocean color and optics in the changing field of operational oceanography. Oceanography 17: 86–95.

———, AND OTHERS. 2004b. Biogeochemical impact of summertime coastal upwelling on the New Jersey Shelf. J. Geophys. Res. 109: C12S02, doi:10.1029/2003JC002265.

GRANT, W. D., AND O. S. MADSEN. 1979. Combined wave and current interaction with a rough bottom. J. Geophys. Res. 87: 1797–1808.

———, A. J. WILLIAMS, AND S. M. GLENN. 1984. Bottom stress estimates and their prediction on the northern California shelf during CODE-1: The importance of wave-current interaction. J. Phys. Oceanogr. 14: 506–527.

HARRIS, C. K., B. BUTMAN, AND P. TRAYKOVSKI. 2003. Wintertime circulation and sediment transport in the Hudson shelf valley. Cont. Shelf Res. 23: 801–820.

JONES, S. C., AND OTHERS. 2003. The extratropical transition of tropical cyclones: Forecast challenges, current understanding, and future directions. Weather Forecasting 18: 1052–1092.

KEEN, T. R., AND S. M. GLENN. 1994. A coupled hydrodynamic-bottom boundary layer model of Ekman flow on stratified continental shelves. J. Phys. Oceanogr. 24: 1732–1749.

———, AND ———. 1995. A coupled hydrodynamic-bottom boundary layer model of storm and tidal flow in the Middle Atlantic Bight of North America. J. Phys. Oceanogr. 25: 391–406.

———, ———, AND R. L. SLINGERLAND. 1994. Coastal circulation and sedimentation during severe storms, p. 279–293. In M. Spaulding [ed.], Third International Conference on Estuarine and Coastal Modeling. American Society of Civil Engineers.

KEIM, B. D., R. A. MULLER, AND G. W. STONE. 2004. Spatial and temporal variability of coastal storms in the North Atlantic Basin. Mar. Geol. 210: 7–15.

KOHUT, J., S. M. GLENN, AND R. CHANT. 2004. Seasonal current variability on the New Jersey inner shelf. J. Geophys. Res. 109: C07S07, doi: 10.1029/2003JC001963.

———, ———, AND J. PADUAN. 2006. The inner-shelf response to tropical storm Floyd. J. Geophys. Res. 111: C09S91, doi: 10.1029/2003JC002173.

LANDRENEAU, D. 2003. Atlantic tropical storms and hurricanes affecting the United States: 1899–2002. NOAA Technical Memorandum NWS SR-206.

MCBRIDE, R. A., AND T. F. MOSLOW. 1991. Origin, evolution, and distribution of shoreface sand ridges, Atlantic inner shelf, U.S.A. Mar. Geol. 97: 57–85.

NIELSEN, J. W., AND R. M. DOLE. 1991. A survey of extratropical cyclone characteristics during GALE. Mon. Weather Rev. 120: 1156–1167.

SANDERS, F., AND J. R. GYAKUM. 1980. Synoptic-dynamic climatology of the "bomb. Mon. Weather Rev. 108: 1589–1606.

SCHLEE, J. S. 1964. New Jersey offshore gravel deposit. Pit Quarry 57: 80–81.

SCHOFIELD, O., T. BERGMANN, W. P. BISSETT, F. GRASSLE, D. HAIDVOGEL, J. KOHUT, M. MOLINE, AND S. GLENN. 2002. Linking regional coastal observatories to provide the foundation for a national ocean observation network. J. Ocean. Eng. 27: 146–154.

———, AND OTHERS. 2007. Slocum gliders: Robust and ready. J. Field Robotics 24: 473–485, doi:10.1002/rob.20200.

SHERWOOD, C. R., R. P. SIGNELL, C. K. HARRIS, AND B. BUTMAN. 2000. Workshop discusses community models for coastal sediment. EOS Trans. Am. Geophys. Union 81: 502.

SKAMAROCK, W. C., J. B. KEMP, J. DUDHIA, D. O. GILL, D. M. BARKER, W. WANG, AND J. G. POWERS. 2005. A description of the Advanced Research WRF version 2. Technical report, National Center for Atmospheric Research, NCAR/TN-468+STR. Available on-line at http://www.mmm.ucar.edu/wrf/users/.

SMITH, J. D., AND S. MCLEAN. 1977. Boundary layer adjustments to bottom topography and suspended sediment, p. 123–151. In J. Nihoul [ed.], Bottom turbulence. Elsevier.

STYLES, R., AND S. M. GLENN. 2000. Modeling stratified wave-current bottom boundary layers for the continental shelf. J. Geophys. Res. 105: 24119–24139.

———, AND ———. 2002. Modeling bottom roughness in the presence of wave-generated ripples. J. Geophys. Res. 107: 3110, doi:10.1029/2001JC000864.

———, AND ———. 2005. Long-term sediment mobilization at LEO-15. J. Geophys. Res. 110: C04S90, doi: 10.1029/2003JC002175.

TRAYKOVSKI, P. 2007. Observations of wave orbital scale ripples and a nonequilibrium time-dependent model. J. Geophys. Res. 112: C06026, doi: 10.1029/2006JC003811.

———, E. HAY, J. D. IRISH, AND J. F. LYNCH. 1999. Geometry, migration, and evolution of wave orbital ripples at LEO-15. J. Geophys. Res. 104: 1505–1524.

TUCKER, M. J., AND E. G. PITT. 2001. Waves in ocean engineering. Elsevier Ocean Engineering Series, London.

TWITCHELL, D. C., AND K. W. ABLE. 1993. Bathymetry, sidescan SONAR image, and surficial geological interpretation of the inner shelf off Little Egg Inlet, New Jersey. U.S. Geological Survey, Miscellaneous Field Studies Map, MF-2221.

WIGGERT, J., B. JONES, T. DICKEY, K. BRINK, R. WELLER, J. MARRA, AND L. A. CODISPOTI. 2000. The northeast monsoon's impact on mixing, phytoplankton biomass, and nutrient cycling in the Arabian Sea. Deep-Sea Res. II 47: 1353–1385.

ZEDLER, S. E., T. D. DICKEY, S. C. DONEY, J. F. PRICE, X. YU, AND G. L. MELLOR. 2002. Analysis and simulations of the upper ocean's response to Hurricane Felix at the Bermuda testbed mooring site: August 13–23, 1995, J. Geophys. Res. 107: 3232, doi:10.1029/2001JC000969.